C: Energy Conversion and Storage; Energy and Charge Transport

A Muon Spectroscopic and Computational Study of the Microscopic Electronic Structure in Thermoelectric Hybrid Silicon Nanostructures

Chenghao Yue, Leandro Liborio, Tiezheng Bian, Simone Sturniolo, Joseph A. Wright, Stephen P. Cottrell, Rustem Khasanov, Gediminas Simutis, Upali Abhaya Jayasooriya, and Yimin Chao

J. Phys. Chem. C, **Just Accepted Manuscript** • DOI: 10.1021/acs.jpcc.9b11717 • Publication Date (Web): 13 Apr 2020

A Muon Spectroscopic and Computational Study of the Microscopic Electronic Structure in Thermoelectric Hybrid Silicon Nanostructures

Chenghao Yue,[†] Leandro Liborio,[‡] Tiezheng Bian,[†] Simone Sturniolo,[‡] Joseph Wright,[†] Stephen P. Cottrell,[§] Rustem Khasanov,[||] Gediminas Simutis,[||] Upali A. Jayasooriya,[†] and Yimin Chao*[†]

[†] School of Chemistry, University of East Anglia, Norwich NR4 7TJ, UK
[‡] Theoretical Computational Physics Group, [§] ISIS Facility, Rutherford Appleton Laboratory, Chilton, Didcot OX11 0QX, UK
[||] Laboratory for Muon Spectroscopy, PSI, CH-5232 Villigen PSI, Switzerland

Supporting Information Placeholder

ABSTRACT: Phenylacetylene capped silicon nanoparticles (Phenyl-SiNPs) have attracted interest as a novel thermoelectric material. Here we report a combined muon spectroscopic (μSR) and computational study of this material in solution to investigate microscopic electronic structure in this system. For comparison, the model molecular compound tetrakis (2-phenylethynyl) silane has also been investigated. μSR measurements have shown that the muon isotropic hyperfine coupling constant, A_μ, which depends on spin density at the muon, is greatly reduced for the Phenyl-SiNPs system when compared to the model compound. Results have also demonstrated that the temperature dependence of A_μ for the Phenyl-SiNPs is of opposite sign and proportionally larger when compared to the model compound. *Ab initio* DFT methods have allowed us to determine the muon addition site in the model compound, while a wider computational study using both DFTB+ and CASTEP offers a qualitative explanation for the reduced coupling seen in the Phenyl-SiNPs system and also the contrasting temperature dependence of A_μ for the two materials. Calculations suggest an increase in the density of electronic states at the energy level of the highest occupied molecular state for the Phenyl-SiNPs, even in the presence of an organic cap, suggesting a mechanism for enhanced electron transport in this system when compared to the tetrakis model compound.

Introduction

Energy shortage and climate change are two of the most serious problems threatening our society. The US Department of Energy (DOE) recognizes thermoelectric technology as one of several potential technological solutions. Specifically, thermoelectric (TE) technology could help to solve the vehicle electrification problem and thus contribute to significantly reducing CO_2 emissions. The DOE continues to commit public money to TE technology development.[1]

A TE device is a solid-state energy converter that converts thermal energy directly into electricity. The efficiency of a TE device depends on the performance of its component materials, and it is embodied in a dimensionless figure of merit ZT, which is given by the following expression:[2]

$$ZT = \frac{\sigma S^2 T}{k} \quad (1)$$

where σ is the electrical conductivity, S is the Seebeck coefficient, k is the thermal conductivity and T is the absolute temperature.

Nanostructured silicon is a promising semiconductor material for thermoelectric devices. Silicon has major advantages in its low cost, relative abundance and low toxicity,[3-4] and many silicon-based materials have been investigated for potential thermoelectric applications.[5-7] In particular, phenylacetylene capped silicon nanoparticles (Phenyl-SiNPs), synthesized via the micelle reduction method,[2, 8] have the potential to become efficient thermoelectric materials, where transport of electrons is possible via conjugated ligands. Because of the characteristic nature of Phenyl-SiNPs, it is possible to improve the electrical conductivity while minimizing thermal conductivity with the same system. Previous characterization measurements for this system provided electric conductivity in the region of 18 $S \cdot m^{-1}$, thermal conductivity 0.1 $Wm^{-1}K^{-1}$ and a Seebeck coefficient of 3228 μVK^{-1} at 300 K.[2]

The experimental work reported here centres on the application of muon spectroscopy (μSR), where beams of 100% spin polarised positive muons are produced by high energy collisions between protons in particle accelerators and stopped in the sample under study. Muons are unstable particles with a mean lifetime of ~2.2 μs, with their decay positrons emitted preferentially in the polarisation direction. The time evolution of the polarisation can therefore be followed with great sensitivity simply by monitoring the time dependence of the decay positron distribution. Muons may thermalize in materials either as the positive muon, with a spin of ½ and a mass of approximately one ninth that of a proton, or may bind an electron

to form muonium (Mu), a light isotope of the H atom. Both species may then undergo further reactions to form alternative diamagnetic or paramagnetic states. Chemically, Mu is almost identical to H and will undergo the same chemical reactions in the sample material. In this experiment it is the addition reaction that is of interest, to form a final state muoniated species.

μSR is a powerful technique that has been used for a wide range of investigations, including magnetic materials,[9] superconductors,[10] functional materials[11] and energy materials,[12] and is a technique that can provide unique information about sample structure and dynamics. In μSR experiments, the local magnetic field felt by the muon is estimated by monitoring the state of the muon spin. When the muon's final state is a paramagnetic muoniated radical, this local magnetic field is dominated by the unpaired electron and the information obtained in the experiment reflects what happens to this electron. Therefore, the μSR technique can be used to study properties such as the dynamics of molecules and radicals,[13] reaction rates[14] and electron transfer/conduction.[15]

A number of muon spectroscopic methods are available, the choice depending on the information required. In this study, both avoided level crossing muon spin resonance (ALC-μSR)[16-17] and transverse field muon spin rotation (TF-μSR) experiments have been carried out.

ALC-μSR is a technique where an external magnetic field is applied along the direction of the muon spin polarisation. This polarisation is monitored as the applied field is scanned, with a loss of polarisation defining a level crossing resonance. Resonances occur when states with opposite muon spin become near-degenerate in energy, and are characterized by the selection rules (ΔM = 0, 1, 2), where M is the quantum number for the z-component of the total angular momentum of the muon, electron, nuclear system. For the case when ΔM = 0 (Δ_0), a muon-proton spin flip-flop, the resonance field ($B^{\Delta 0}$) given by the formula below:[5]

$$B^{\Delta_0} = \frac{1}{2}\left|\frac{A_\mu - A_p}{\gamma_\mu - \gamma_p} - \frac{A_\mu + A_p}{\gamma_e}\right| \qquad (2)$$

These resonances are seen for radicals in solid, liquid and gaseous phases, where for isotropic media A_μ and A_p are the isotropic muon and proton hyperfine coupling constants (in MHz), and can be used to estimate the vibrationally averaged electron spin density at the nucleus,[18] while γ_μ, γ_p, and γ_e are the muon, proton, and electron gyromagnetic ratios, 135.5 MHz T^{-1}, 42.57 MHz T^{-1}, and 2.8025×10^4 MHz T^{-1}, respectively.[18] Since the peak position is related to the hyperfine couplings of the muon and the proton in the radical, and the hyperfine coupling constants are characteristic of a particular muoniated radical, one can use these lines for assigning the observed resonances to a particular radical species.[19] A muon spin flip transition, ΔM = 1 (Δ_1), may also be observed; however, in the absence of anisotropy (as for these compounds in solution) this resonance will be absent.[5]

In our previous work,[20] the ALC-μSR technique was employed to investigate Phenyl-SiNPs system in the solid state. These preliminary measurements showed clear resonance lines around 2.2 T for both the Phenyl-SiNP and model molecular compound, with a reduction in the resonance line width above room temperature, suggesting an activated behaviour for the system.[20] *Ab* initio DFT simulations were carried out to calculate the hyperfine parameters for the model molecular system. Predictions suggested a radical species being formed with a value for $A_\mu \sim 400$ MHz by the addition of muonium to the carbon C7, with the measured lines corresponded to Δ_0 resonances associated with protons on the Phenyl ring. Curiously, the associated Δ_1 resonances appeared to be weak and very broad, and difficult to reliably determine from the baseline. We therefore decided to continue the study by investigating both systems in solution, where motional averaging would be expected to give narrow lines and better resolution of radical species for ALC-μSR measurements, while allowing A_μ to be straightforwardly determined by carrying out a TF-μSR measurement.

For TF-μSR measurements, relatively high fields are used that fall within the so-called Paschen-Back regime. The frequency spectrum of a system under these circumstances is typically characterised by a single peak at the muon's Larmor precession frequency seen for all diamagnetic muon states. This peak is known as a diamagnetic peak, and it appears together with a pair of resonance peaks placed approximately symmetrically about this diamagnetic peak. The value of A_μ can simply be determined from the splitting between these two satellite lines. Specific muon analysis software, WIMDA, was used to correlate these line pairs in the measured data to obtain values for A_μ.[21]

Knowledge of the microscopic conduction rates and mechanisms in these materials would be useful in our attempt to improve these materials by design. μSR has been shown to be an elegant method for measuring microscopic conduction rates and mechanisms in conducting organic polymers,[15] which are materials structurally similar to the ligands found in phenylacetylene functionalized SiNPs. Further, muonium adducts to carbon-carbon triple bonds in other organic compounds have already been characterized.[22]

In this work, Phenyl-SiNPs in solution state are investigated by both ALC-μSR and TF-μSR, while a solution of the model compound tetrakis (2-phenylethynyl) silane is employed as a reference for comparison. Key to interpreting the data has been the extended computational modelling, allowing us to assign the Mu addition site in these systems and to gain insight into the electronic structure of the Phenyl-SiNPs. The results have enabled us to propose a mechanism for the thermoelectric behaviour seen in these materials.

Experimental

Synthesis of Tetrakis (2-Phenylethynyl) Silane

Phenylacetylene and n-Buty-lithium were added to distilled tetrahydrofuran (THF) and stirred for 30 min to give a yellow suspension. This suspension was added to a fully dispersed solution of silicon tetrachloride in THF and was refluxed overnight. The residue was filtered and dissolved in toluene, filtered and dried to get the model compound. Recrystallisation using dichloromethane gave white needle-like microcrystals.

Synthesis of Phenylacetylene capped silicon nanoparticles

A mixture of sodium metal and naphthalene were sonicated for two hours in distilled THF and immediately added to the fully dispersed solution of silicon tetrachloride in THF to give a white cloudy suspension. Tetrakis (2-Phenylethynyl) silane was added to the reaction medium and refluxed for 8 hours. Deionized water was added to the final solution to react with any surplus lithium. The organic layer was evaporated to give a yellow-orange powder. The residue was heated in an oil bath and pumped under vacuum to remove the residual naphthalene. The final product was an orange crystalline solid powder.

FTIR

The FTIR spectra were collected using a Perkin-Elmer 100 ATR FTIR spectrometer. The solid sample was placed on the crystal to take the measurement and the background was corrected by taking a spectrum of the clean crystal.

μSR

The ALC-μSR measurements were undertaken using the HIFI spectrometer at the ISIS muon facility of the Rutherford Appleton Laboratory (RAL), Oxfordshire, UK,[23] while the TF data was measured using the GPD spectrometer at the Paul Scherrer Institute (PSI), Villigen, near Zurich, Switzerland.[24] Samples were redissolved in spectroscopic grade THF with concentrations of 200 mM for the model compound and 115 mg/ml for the SiNPs. At least three cycles of freeze-pump-thaw were carried out to remove O_2 in the solution. For measurements at ISIS, the solutions were loaded into titanium sample cells (with a 35 mm diameter foil beam window) inside a glovebox purged with high purity argon. The sample environment was provided by a closed cycle refrigerator. At PSI, a high momentum muon beam was available, and samples were sealed immediately after degassing in a glass sample holder, which was placed directly in a gas flow cryostat. In both experiments, the temperature range available for the study was limited by the freezing and boiling points of the THF solvent.

Computer Simulations

Computer simulations were used for interpreting data measured for radicals formed by muonium addition. The muon stopping sites in both the model compound and the Phenyl-SiNPs were studied using Density Functional Tight Binding (DFTB) calculations, as implemented in the DFTB+ code,[25] and standard DFT calculations, as implemented in the CASTEP code (see supporting information).[26] The combination of these computational results with the ALC-μSR and TF-μSR experimental data provides a unique insight into electronic structure of these materials.

In the case of the model compound, there are eight possible sites of addition for Mu in each of the phenylacetylene molecules bonded to the silicon atom, which might result in potentially eight different organic radicals. These radicals might be computationally distinguishable from one another depending on the symmetry of the system. As regards the Phenyl-SiNPs, the potential addition sites for Mu are in the same phenylacetylene molecules, which are now attached to the silicon nanoparticles.

The molecular structure of the model compound, with its potential muon addition sites indicated in red, is shown in Figure 1. The eight potential addition sites for Mu correspond to all the regions of unsaturation in the organic ligand. When Mu reacts with one of these unsaturated centres, it forms a muoniated radical, which has an unpaired electron that may be distributed throughout the molecule and may interact with the muon by the hyperfine coupling. In this work, the focus was placed on the calculation of the Fermi contact term part of the hyperfine tensor, A_μ, which can be compared to experimental results.

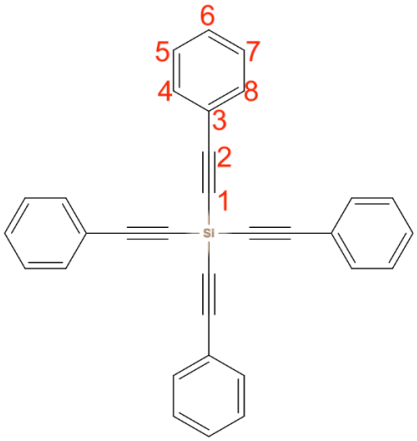

Figure 1. The tetrakis (2-phenyethynyl) silane molecule with the potential muon addition sites shown in red.

In contrast, applying similar DFT codes to study the Phenyl-SiNP system is computationally difficult. The mean diameter of the experimentally produced Phenyl-SiNPs is 6 nm and the surface ligands occupy 25 wt% estimated from TGA data obtained in our previous work;[2] however, nanoparticles of this size are well beyond the simulation capabilities of current DFT codes. Hence, it was necessary to develop an adequate model for the Phenyl-SiNP that was large enough to represent the properties that were experimentally observed and yet small enough to be computationally manageable (see supporting information).

To test this methodology, a series of calculations on Si nanoparticles of different sizes, with different numbers of muoniated ligands attached to them, were performed. The model nanoparticles were built by using the Wulff construction method,[25, 27] and given a certain target radius. Their geometry was relaxed with DFTB+, the ligands were attached radially to some surface atoms, and the geometry was relaxed again. Finally, for the systems simulated with CASTEP, the geometry was relaxed a third time to compensate for the small differences in potential between DFT and DFTB+ calculations. Particles were generated with radii between 3 and 6 Å, and with 1 to 5 organic ligands attached to them. Figure 2 and 3 show the schematic pictures of the type of systems that were simulated.

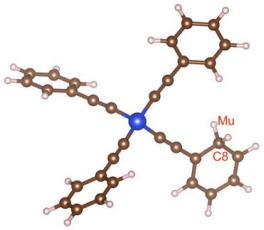

Figure 2. Muonated tetrakis (2-phenyethynyl) silane molecule, with the muon on C8.

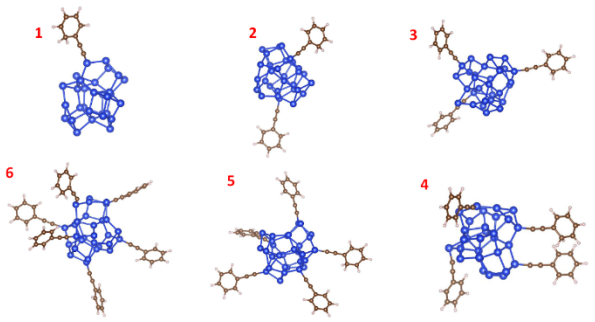

Figure 3. Nanoparticle systems simulated with DFTB+, to determine an appropriate nanoparticle size to be simulated with CASTEP. The sequence shows how different systems were constructed with differing numbers of organic ligands attached.

These initial calculations were carried out with the DFTB+ code because it allows for the efficient treatment of relatively large systems. The modelled nanoparticles proved to have well-converged electronic charges in their organic ligands and their hydrogen atoms and were relaxed reasonably fast. The average Mulliken charges for the whole organic ligands and for the hydrogens in the organic ligands were converged with respect to the size of the Si nanoparticle and the number of organic ligands attached to it (see supporting information). Since the aim was to investigate the changes in the values of A_μ in both the model compound and the Phenyl-SiNPs, it was important to secure a size for the Phenyl-SiNPs that would not introduce size-related effects into the electronic densities of the hydrogens and the attached muon, which are related to the value of A_μ. Hence, nanoparticles of 6 Å. with six ligands were adopted as the systems used to simulate the Phenyl-SiNPs.

DFTB+, however, does not have a module to calculate values of hyperfine coupling tensors. Hence, to investigate the changes in values of A_μ for the muon in the model compound and the Phenyl-SiNPs, CASTEP calculations were also performed on a 6 Å Phenyl-SiNPs with six ligands attached to them. Modelling of the 6 Å. Phenyl-SiNPs was carried out with the muon placed on the same carbon as determined to be the addition site for the model compound.

Results and discussion

FTIR spectra provide evidence of successful capping of SiNPs with phenylacetylene. In Figure 4, the data shows a peak at 3052 cm^{-1} which is characteristic of aromatic C-H bonds. The peaks at both 1596 and 1487 cm^{-1} are indicative of aromatic C-C bonds. Also, the clearly visible sharp peak at 2159 cm^{-1} is characteristic of the C≡C bond, suggesting that the terminal side of the alkyne is attached to silicon. Further supporting evidence are the peaks characteristic of Si-C≡C at 1451 and 1220 cm^{-1}. The model compound has the same rings attached to silicon, and its features are, therefore, similar to those of the SiNPs, see the inset in Figure 4.

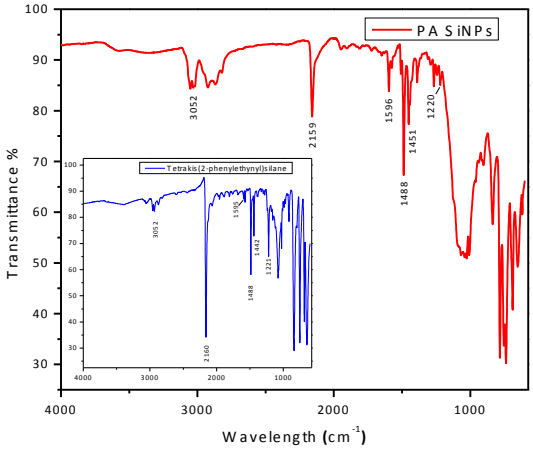

Figure 4. FTIR of phenylacetylene capped SiNPs, Inset, FTIR of tetrakis (2-phenylethynyl) silane, both obtained using an ATR FTIR spectrometer.

The Fermi contact term for the muon, A_μ, can be directly determined from the high transverse field (TF-μSR) experiments. Figures 5 (a) and (b) show representative frequency correlation spectra at 300 K for the Phenyl-SiNPs and the model compound, respectively. The peak position indicates the value of A_μ. Figures 5 (c) and (d) show the temperature dependence of A_μ for the two compounds. From the TF-μSR spectra shown in Figures 5 (a) and (b), it can be seen that the peak positions at 300 K are around 350 MHz for Phenyl-SiNPs and around 450 MHz for the model compound. However, as the temperature increases, the TF-μSR peaks for the Phenyl-SiNPs move towards lower frequency values, whereas those for the model compound move slightly towards higher frequency values. From linear fits to the data shown in Figures 5 (c) and (d), one can see that the gradients are -0.08 MHz/K and 0.036 MHz/K for the Phenyl-SiNPs and model compound, respectively. This corresponds to a change in A_μ for Phenyl-SiNPs and model compound of approximately 10 MHz and 4 MHz, respectively, measured over a similar temperature range.

Changes in A_μ are therefore not only opposite in value, they are also very different in size, with that for the Phenyl-SiNPs being considerably more signifcant. Correlation spectra for all the temperatures considered are displayed in Figure S1 in the supporting information.

Table 1. Calculated values for the Fermi contact term (A_μ) for the muon in the addition sites 1-8 of the structurally relaxed model compound. The values of A_μ do not include dynamical corrections.

Sites	Contact Term A_μ (MHz)
1	483.89
2	530.82
3	517.88
4	423.03
5	504.20
6	380.04
7	508.30
8	436.59

To provide insight as to the Mu addition site in these materials, computer simulations have been carried out to calculate the Fermi contact terms, A_μ, for Mu addition to sites 1-8 of the model compound. Results are shown in Table 1.

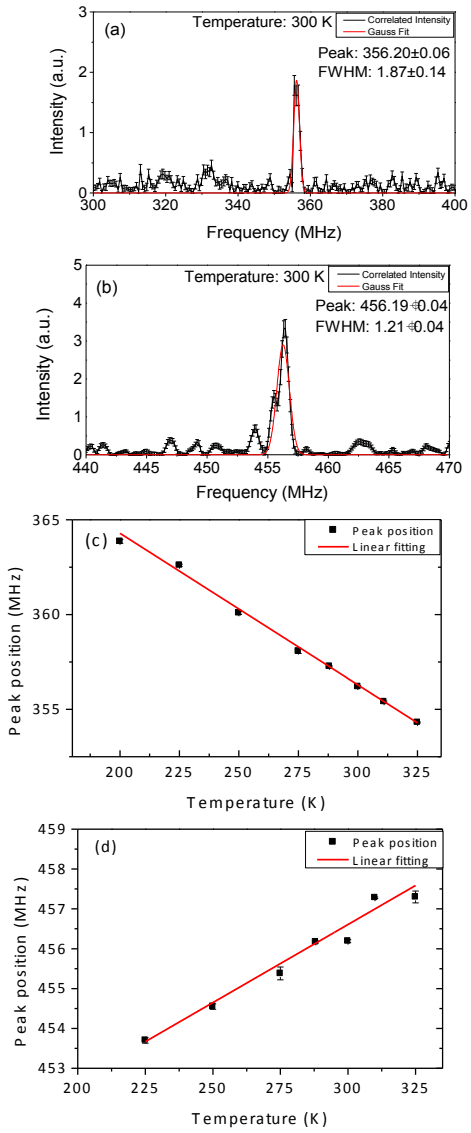

Figure 5. TF-μSR frequency correlation spectra for Phenyl-SiNPs (a) and tetrakis (2-phenylethynyl) silane (b) at 300 K. The temperature dependance of A_μ is shown for Phenyl-SiNPs (c) and tetrakis (2-phenylethynyl) silane (d). For the Phenyl-SiNPs, A_μ decreases by ~10 MHz with increasing temperature, suggesting a ~3% reduction in the unpaired spin density at the muon site. In contrast, for the model compound, A_μ increases by ~4 MHz for a similar temperature step, representing an increase in the unpaired spin density at the muon of <1%.

The comparison of these calculated values with the experimental results from TF-μSR (Figure 5), suggests that Mu is likely to be attached at position C8 in the model compound (see Figure 1). The values obtained from the experimental results from TF-μSR also allow us to rule out the addition of the muon to any part of the silicon nanoparticle. Table 2 presents and compares the CASTEP results obtained for the model compound and the 6 Å Phenyl-SiNPs. It can be seen that, in agreement with the experimental results, the computed value of A_μ for the Phenyl-SiNPs is smaller than the computed value of A_μ for the model compound. The modelling results also show that this decrease in the value of the A_μ is correlated with a decrease in the total electronic and spin populations at the muon site when we go from the model compound to the Phenyl-SiNPs.

ALC-μSR results for both the Phenyl-SiNPs and the model compound are shown in Figure 6. Clear Δ_0 resonances are seen, associated with addition of Mu to the ring at position C8 and the coupling to ring protons. Interesting temperature effects, including line broadening and a shift in the resonance peak with temperature, have been measured. Figures 6 (a) and (b) show representative ALC-μSR spectra measured at 300K for the Phenyl-SiNPs and model compound, respectively. Gaussian fitting to the lines shown in the Figure was performed using the Mantid analysis software.[28] The ALC-μSR resonances are observed at values of the magnetic field of around 1.75 T for the Phenyl-SiNPs and at around 1.65 T for the model compound.

Assignment of the ALC peaks, and the implication this has on our understanding of spin density across the molecule, can be investigated by combining the TF-μSR measurement of A_μ (Figure 5) with the results of the ALC-μSR study (Figure 6), to determine values for A_p from Equation 2. For the Δ_0 lines measured at 300K, calculations performed using the experimental results give values for A_p of 28.7 MHz and 147.9 MHz for the Phenyl-SiNPs and the model compound, respectively. Experimental values, calculated in the same manner, at other temperatures, are given in the supporting information. Insight into this surprising difference in the values of A_p determined from experimental data for the two systems is provided by DFT calculations and is shown in Table 3. The signs of the calculated values for A_p are relative to the initial spin polarisation chosen for the muon at the beginning of the DFT calculation, i.e. a change in the sign of the initial spin polarisation would cause all signs to flip. However, considering the sign convention adopted in this work, the experimentally calculated values of A_p for the Phenyl-SiNPs (28.7 MHz) and the model compound (147.9 MHz) can be associated with the values of -25.54 MHz for site 5 in the Phenyl-SiNPs, and with the value of 129.85 MHz for site 8 in the model compound. Hence, the values in Table 3 show that while the Δ_0 line measured close to 1.65 T for the model compound arises from hyperfine coupling of electrons with the ipso-proton, the Δ_0 line measured close to 1.77 T for the Phenyl-SiNPs is instead likely to be due to the hyperfine coupling of electrons with the ring proton bonded to C5 in Figure 1. Table 3 also shows that the values of A_p, due to the hyperfine coupling of electrons with all the protons in the ring, are reduced in the Phenyl-SiNPs with respect to the model compound: a result that is consistent with the earlier conclusion that there is a reduced unpaired spin density in the Phenyl-SiNPs.

The temperature dependence of these ALC-μSR resonance peaks in the range 200 K to 325 K are shown in Figure 6 (c) and (d) for the Phenyl-SiNPs and model compound, respectively. Very similar trends with temperature are observed for the two compounds, with the peak position moving to lower fields as the temperature is increased. From linear fits to the data, shown in Figures 6 (c) and (d), gradients of -2.7 G/K and -2.2 G/K are determined for the Phenyl-SiNPs and model compound, respectively. Parameters obtained from fitting the ALC spectra at all temperatures are presented in Figure S2 of the supporting information.

Table 2. CASTEP results for the tetrakis (2-phenylethynyl) silane and the Phenyl-SiNPs with Mu added at carbon atom C8. The charges and spin densities shown were computed at the Mu position and are expressed in atomic units (a. u.).

System	Total Mulliken population (a. u.)	α Mulliken spin population (a.u.)	β Mulliken spin population (a.u.)	Total Mulliken spin population (a.u.)	A_μ (MHz)
6 Å Phenyl-SiNPs	0.680	0.360	0.320	0.040	323.97
Tetrakis (2-phenylethynyl) silane	0.694	0.388	0.322	0.066	436.59

There is a distinct change in the form of the ALC spectra observed between 300 K and 325 K for the model compound. Strikingly, at the higher temperature, the intensity of the resonance peak more than doubles, while the width is reduced by approximately one third. In contrast, all other temperatures appear to show very similar resonances to within the signal to noise of the present data. This observed change for the model compound is thought likely to be due to differences in dynamics of the two samples, particularly the barrier to rotation of the phenyl group, which is dependent on the bond order of the bonds between the phenyl ring and the nanoparticle or the Si atom in the model compound. Even though one tends to write these chemical formulae with the bonds between the phenyl ring and the silicon centre as a single bond followed by a triple bond and another single bond, the bond order in reality will be different due to any delocalisation of electrons. The difference in A_μ suggests a smaller amount of delocalisation of the unpaired electron in the model compound compared to the Phenyl-SiNPs, one would expect a higher barrier to phenyl rotation in the case of the nanoparticle compared to the model compound. Therefore, it is likely that we are observing this energy barrier around 325 K in the case of the model compound, while that for the Phenyl-SiNPs this would be predicted to be at higher temperatures.

Table 3. Calculated theoretical values of the isotropic hyperfine couplings of the protons with electrons, A_p, for protons bonded to the addition sites 4-8. The muon is attached to site 8. The negative and positive signs of these values are relative to the initial spin polarisation chosen for the muon in the DFT calculations.

Sites	A_p Model Compound (MHz)	A_p Phenyl-SiNPs (MHz)
4	8.164	7.35
5	-29.78	-25.54
6	6.490	5.62
7	-22.24	-18.852
8	129.85	127.26

The TF-μSR measurements shown in Figure 5 provide values for A_μ that allow an estimate of the unpaired electron density at the muon site. These experiments show that the trends with temperature, for the values of A_μ in the model compound and the Phenyl-SiNPs, are different. In the case of Phenyl-SiNPs, the value of A_μ decreases by 10 MHz with increasing temperature, which indicates a decrease in the unpaired electronic density at the muon site. In the case of the model compound, A_μ increases by only 4 MHz. The decrease in unpaired electron density at the muon site with decreasing temperature for the Phenyl-SiNPs may be interpreted as an increase in conduction away from the muon site, which is similar to what is observed for conduction in metals, due to a reduction in the phonon excitations.[29]

To investigate this phenomenon further, we used computational modelling to propose a plausible model for the experimentally observed effects of the temperature on the values of A_μ in the model compound and the muoniated Phenyl-SiNPs.

Figure 7 shows the calculated electronic energy states of the model compound (left) and those of the muoniated 6 Å Phenyl-SiNPs with six ligands attached to it (right). These calculations were carried out with CASTEP. The red and blue vertical stripes represent the electronic energy states for the α and β spin channels and the grey vertical stripes represent the unoccupied electronic energy states in both channels. The black plots superimposed on these electronic energy states represent the projected electronic density of states (PDOS) associated to the muon, namely which is obtained in CASTEP by projecting the total density of states onto the orbitals associated with the muon.[30] Hence, this PDOS is connected to the spatial distribution of the spin density associated with the muon.

The electronic structure of the model compound shows a peak on the PDOS associated to the muon at the energy level of the highest occupied molecular state in both channels, which indicates that there is a strong component of muon states at those energy levels. As the muoniated model compound tetrakis (2-phenylethynyl) silane is a radical, we can identify a singly occupied molecular orbital (SOMO) that is associated with the unpaired electron density at the muon site. This high electron density at the muon site is what explains the relatively large values of the A_μ in this model compound.

Furthermore, the electronic structure of the model compound shows a minimum energy-gap, between occupied and unoccupied states, of approximately 1 eV in the down spin channel. No sensible increase in temperature will be able to allow the electrons in the SOMO to jump to the next energy levels and, therefore, the value of the A_μ of the muon is unlikely to go down.

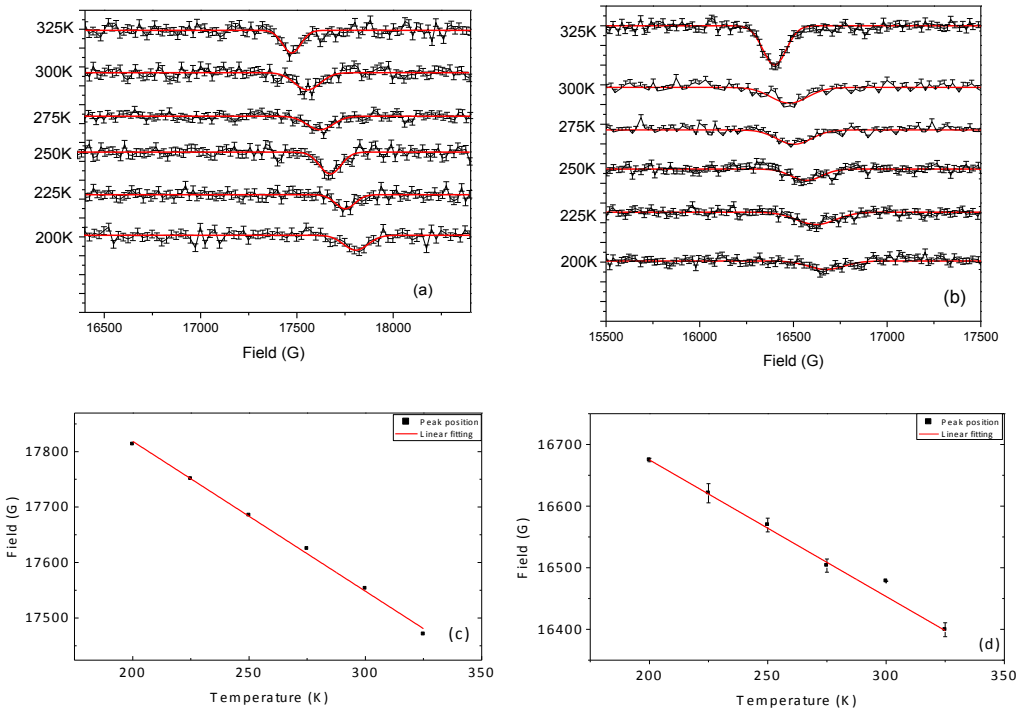

Figure 6. ALC-μSR, showing clear Δ_0 lines for Phenyl-SiNPs (a) and tetrakis (2-phenylethynyl) silane (b). The temperature dependence of the resonance peak position for Phenyl-SiNPs (c) and tetrakis (2-phenylethynyl) silane (d). Note that for the Phenyl-SiNPs the Δ_0 line likely arises from coupling to the ring proton bonded to C5 in Figure 1, while for the model compound coupling is to the ipso-proton.

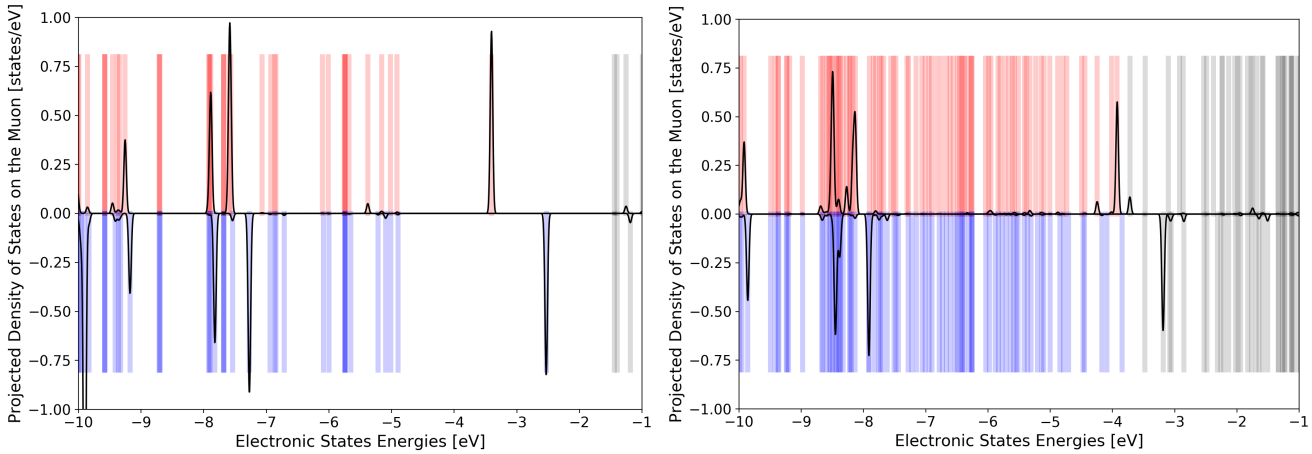

Figure 7. The calculated electronic energy states of the tetrakis (2-phenylethynyl) silane muoniated molecule (left) and those of the muoniated 6 Å Phenyl-SiNPs with six ligands attached (right). The red and blue vertical stripes represent the occupied electronic energy states for the α and β spin channels. The grey vertical stripes represent the unoccupied electronic energy states in both channels. The black plots superimposed on these electronic energy states represent the projected electronic states associated to the muon.

As regards the muoniated Phenyl-SiNPs, their electronic energy states are closer together in energy in its electronic structure. We expect these discrete states to come closer, reach a continuum and become energy bands as the nanoparticles get bigger and more bulk-like, since metallic behaviour at the surface of Si nanoparticles is a known phenomenon.[31] Regarding the projected density of states associated with the muon in the muoniated Phenyl-SiNP, this is not exclusively at the energy level of the highest occupied molecular state anymore, rather it is smeared above and below the energy of this highest occupied molecular level. This combination of distributed muon states and the phenyl-SiNPs having their electronic energy states closer together helps to explain why A_μ for muoniated Phenyl-SiNPs is smaller than in the model compound.

The electronic structure of the muoniated Phenyl-SiNPs system may also offer a qualitative explanation of the temperature dependence of A_μ. For the real nanoparticles, the energy states around the energy level of the highest occupied molecular state

will likely form a continuum of energy bands and, as the temperature increases, it would be easier for an electron in a band close to that energy level to jump to the next energy level, as the levels will all be quite close to each other. If the new occupied level had a smaller contribution to the hyperfine coupling it would end up reducing the total coupling. However, this process would need to be considered alongside effects arising from molecular dynamics, which have not yet been investigated for this system.

This model for the electronic structure for the two systems also helps explain the form of the ALC-μSR spectra presented in Figure 6. The electronic structure of the Phenyl-SiNPs is correlated with a larger electronic delocalisation of its unpaired electron when compared to the unpaired electron in the tetrakis (2-phenylethynyl) silane model compound, whose electronic structure has a relatively large energy-gap between occupied and unoccupied states that would make electronic delocalisation more difficult. The larger electronic delocalisation in the Phenyl-SiNPs can affect the the bonds between the phenyl ring and the Si nanoparticle: rather than having a single-triple-single bond order, the electronic delocalisation may produce a different bond order that will likely affect the single bonds and increase the energy barrier for the phenyl rotation in the Phenyl-SiNPs, which is what is observed in the ALC-μSR results presented in Figure 6. Table 4 shows the lengths of these single-triple-single bonds between the phenyl ring that has the attached muon and the Si atom where the organic ligand attaches to. It can be seen that, when going from the model compound to the Phenyl-SiNPs, the single bonds between Si-C1 and C2-C3 get shorter, while the triple bond between C1-C2 get longer. This is an indication that the single-triple-single bonds may be turning into double-double-double bonds, which may make the phenyl rotation more difficult.

Table 4. Change in the lengths of the bonds that link the phenyl ring to a silicon atom in both the model compound and the Phenyl-SiNPs. The change in the bond lengths indicates an increased energy barrier for phenyl ring rotation in the Phenyl-SiNPs.

Bond	Bond length model compound (Å)	Bond lenght Phenyl-SiNPs (Å)	Change in Bond length (Å)
Si-C1	1.817	1.812	-0.005
C1-C2	1.232	1.239	0.007
C2-C3	1.399	1.389	-0.01

Conclusions

In summary, μSR measurements have shown that there is a difference in the electronic structure of the Phenyl-SiNPs and the tetrakis (2-phenylethynyl) silane model compound. In particular, the experimental results demonstrate that the spin density on the muon is significantly reduced for the Phenyl-SiNPs system compared to the model compound. The low temperature values of A_μ are of the order of 450 MHz and 350 MHz for the model compound and the Phenyl-SiNPs, respectively. Furthermore, the changes of the relative values of A_μ with temperature in the Phenyl-SiNPs are significantly larger than in the model compound. ALC measurements confirm the reduction of unpaired spin density in the Phenyl-SiNPs, and suggest a future study to create a detailed map of unpaired spin density across this molecular system.

Compared to our previous work studying polycrystalline samples, measurements of the two systems in solution show a significantly greater separation in hyperfine parameters (based on the shift to low field of the ALC line positions for the Phenyl-SiNPs). Further study would be of merit; however, this may be complicated by broad lines and the difficulty of determining A_μ directly in the solid.

A computational study using both DFTB+ and CASTEP supports these results, while also offering a qualitative explanation for the change in the bonding between the Si nanoparticles and the phenyl rings, and for the temperature dependence of A_μ in both the Phenyl-SiNPs and the model compound. Calculations indicate that the Phenyl-SiNPs have electronic states that are closer in energy than those in the model compound. This variation in the electronic structure of both systems suggests a mechanism for the temperature dependence of the values of A_μ in the model compund and the Phenyl-SiNPs system.

This combined μSR and computation study has therefore provided insight into the processes that affect the microscopic electronic structure of these systems. By contrasting results from the Phenyl-SiNPs and the tetrakis model compound we have gained an insight into how the electronic properties are modified by incorporating a Si NP into the molecular system.

ASSOCIATED CONTENT

Supporting Information

The following Supporting Information is available free of charge on the ACS Publications website: TF-μSR data, ALC data, Calculated A_P values for the experimentally observed Δ_0 lines, Technical details for the computer simulations.

AUTHOR INFORMATION

Corresponding Author

Email: y.chao@uea.ac.uk
Email: leandro.liborio@stfc.ac.uk

Notes

The authors declare no competing financial interests.

Acknowledgements

Experiments at the ISIS Pulsed Neutron and Muon Source were supported by a beamtime allocation from the Science and Technology Facilities Council (RB1820054; RB1620403; RB1520478); We acknowledge the Paul Scherrer Institut, Villigen, Switzerland for provision of Muon beamtime at GPD, and EPSRC for travel grant (EP/P020178/1). We also acknowlegde the computational support provided by (a) STFC Scientific Computing Departments SCARF cluster; and (b) the UK Materials and Molecular Modelling Hub for computational resources, which is partially funded by EPSRC (No. EP/P020194/1). Funding for the simulation work was provided by the STFC-ISIS muon source and by the CCP for NMR Crystallography, funded by EPSRC Grant Nos. EP/J010510/1 and EP/M022501/1.

Reference:

(1) Hendricks, T.; Choate, W. T., *Engineering Scoping Study of Thermoelectric Generator Systems for Industrial Waste Heat Recovery*; US Department of Energy: 2006; pp 1-74.
(2) Ashby, S.; Thomas, J. A.; Garcia-Canadas, J.; Min, G.; Corps, J.; Powell, A. V.; Xu, H.; Shen, W.; Chao, Y., Bridging Silicon Nanoparticles and Thermoelectrics: Phenylacetylene Functionalization. *Faraday Discuss.*

2014, *176*, 349-361.
(3) Kang, Z.; Liu, Y.; Lee, S. T., Small-Sized Silicon Nanoparticles: New Nanolights and Nanocatalysts. *Nanoscale* **2011,** *3* (3), 777-791.
(4) Buriak, J. M., Organometallic Chemistry on Silicon and Germanium Surfaces. *Chem. Rev.* **2002,** *102* (5), 1271-1308.
(5) McKenzie, I., The Positive Muon and [Small Mu]Sr Spectroscopy: Powerful Tools for Investigating the Structure and Dynamics of Free Radicals and Spin Probes in Complex Systems. *Annu. Rep. Prog. Chem., Sect. C: Phys. Chem.* **2013,** *109* (0), 65-112.
(6) Hochbaum, A. I.; Chen, R. K.; Delgado, R. D.; Liang, W. J.; Garnett, E. C.; Najarian, M.; Majumdar, A.; Yang, P. D., Enhanced Thermoelectric Performance of Rough Silicon Nanowires. *Nature* **2008,** *451*, 163-167.
(7) Boukai, A. I.; Bunimovich, Y.; Tahir-Kheli, J.; Yu, J. K.; Goddard, W. A.; Heath, J. R., Silicon Nanowires as Efficient Thermoelectric Materials. *Nature* **2008,** *451*, 168-171.
(8) Baldwin, R. K.; Pettigrew, K. A.; Garno, J. C.; Power, P. P.; Liu, G.-y.; Kauzlarich, S. M., Room Temperature Solution Synthesis of Alkyl-Capped Tetrahedral Shaped Silicon Nanocrystals. *J. Am. Chem. Soc.* **2002,** *124* (7), 1150-1151.
(9) Réotier, P. D. d.; Yaouanc, A., Muon Spin Rotation and Relaxation in Magnetic Materials. *J. Phys.: Condens. Matter* **1997,** *9*, 9113.
(10) Uemura, Y. J., Muon Spin Relaxation Studies on High - Tc Superconductors and Related Antiferromagnets (Invited). *J. Appl. Phys.* **1988,** *64* (10), 6087-6091.
(11) Drew, A. J.; Hoppler, J.; Schulz, L.; Pratt, F. L.; Desai, P.; Shakya, P.; Kreouzis, T.; Gillin, W. P.; Suter, A.; Morley, N. A.; Malik, V. K.; Dubroka, A.; Kim, K. W.; Bouyanfif, H.; Bourqui, F.; Bernhard, C.; Scheuermann, R.; Nieuwenhuys, G. J.; Prokscha, T.; Morenzoni, E., Direct Measurement of the Electronic Spin Diffusion Length in a Fully Functional Organic Spin valve by Low-Energy Muon Spin Rotation. *Nat. Mater.* **2009,** *8* (2), 109-114.
(12) Sugiyama, J.; Nozaki, H.; Umegaki, I.; Mukai, K.; Miwa, K.; Shiraki, S.; Hitosugi, T.; Suter, A.; Prokscha, T.; Salman, Z.; Lord, J. S.; Månsson, M., Li-Ion Diffusion in Li4ti5o12 and Liti2o4 Battery Materials Detected by Muon Spin Spectroscopy. *Phys. Rev. B* **2015,** *92* (1), 014417.
(13) McKenzie, I.; Scheuermann, R.; Sedlak, K.; Stoykov, A., Molecular Dynamics in Rod-Like Liquid Crystals Probed by Muon Spin Resonance Spectroscopy. *J. Phys. Chem. B* **2011,** *115* (30), 9360-9368.
(14) Walker, D. C., *Muon and Muonium Chemistry*. Cambridge University Press: Cambridge, 1983.
(15) Pratt, F. L., Muon Spin Relaxation as a Probe of Electron Motion in Conducting Polymers Muon Spin Relaxation as a Probe of Electron Motion In. *J. Phys.: Condens. Matter* **2004,** *16*, S4779.
(16) Abragam, A., Spectrometry through Level-Crossing in Muon Physics. *C. R. Acad. Sci., Ser. II* **1984,** *299* (3), 95-99.
(17) Kiefl, R. F.; Kreitzman, S.; Celio, M.; Keitel, R.; Luke, G. M.; Brewer, J. H.; Noakes, D. R.; Percival, P. W.; Matsuzaki, T.; Nishiyama, K., Resolved Nuclear Hyperfine-Structure of a Muonated Free-Radical Using Level-Crossing Spectroscopy. *Phys. Rev. A* **1986,** *34* (1), 681-684.
(18) Roduner, E.; Stolmár, M.; Dilger, H.; Reid, I. D., Reorientational Dynamics of Cyclohexadienyl Radicals in High-Silica Zsm-5. *J. Phys. Chem. A* **1998,** *102* (39), 7591-7597.
(19) Clayden, N. J., Muons in Chemistry. *Phys. Scr.* **2013,** *88* (6), 068507.
(20) Bian, T.; Peck, J. N.; Cottrell, S. P.; Jayasooriya, U. A.; Chao, Y., Hybrid Silicon Nanostructures with Conductive Ligands and Their Microscopic Conductivity. *J. Electron. Mater.* **2017,** *46* (5), 3221-3226.
(21) Pratt, F. L., Wimda: A Muon Data Analysis Program for the Windows PC. *Phys. B* **2000,** *289*, 710-714.
(22) Oganesyan, V. S.; Cammidge, A. N.; Hopkins, G. A.; Cotterill, F. M.; Reid, I. D.; Jayasooriya, U. A., Muon Spin Rotation Studies of Enediynes. *J. Phys. Chem. A* **2004,** *108* (10), 1860-1866.
(23) Lord, J. S.; McKenzie, I.; Baker, P. J.; Blundell, S. J.; Cottrell, S. P.; Giblin, S. R.; Good, J.; Hillier, A. D.; Holsman, B. H.; King, P. J. C.; Lancaster, T.; Mitchell, R.; Nightingale, J. B.; Owczarkowski, M.; Poli, S.; Pratt, F. L.; Rhodes, N. J.; Scheuermann, R.; Salman, Z., Design and Commissioning of a High Magnetic Field Muon Spin Relaxation Spectrometer at the Isis Pulsed Neutron and Muon Source. *Rev. Sci. Instrum.* **2011,** *82* (7), 073904.
(24) Khasanov, R.; Guguchia, Z.; Maisuradze, A.; Andreica, D.; Elender, M.; Raselli, A.; Shermadini, Z.; Goko, T.; Knecht, F.; Morenzoni, E.; Amato, A., High Pressure Research Using Muons at the Paul Scherrer Institute. *High Pressure Res.* **2016,** *36* (2), 140-166.
(25) Porezag, D.; Frauenheim, T.; Köhler, T.; Seifert, G.; Kaschner, R., Construction of Tight-Binding-Like Potentials on the Basis of Density-Functional Theory: Application to Carbon. *Phys. Rev. B* **1995,** *51* (19), 12947-12957.
(26) Clark, S. J.; Segall, M. D.; Pickard, C. J.; Hasnip, P. J.; Probert, M. J.; Refson, K.; Payne, M. C., First Principles Methods Using Castep. *Z. Kristallogr. Cryst. Mater.* **2005,** *220* (5-6), 567-570.
(27) Wulff, G., XXV. Zur Frage Der Geschwindigkeit Des Wachsthums Und Der Auflösung Der Krystallflächen. *Z. Kristallogr. Cryst. Mater.* **1901,** *34*, 449-530.
(28) Arnold, O.; Bilheux, J. C.; Borreguero, J. M.; Buts, A.; Campbell, S. I.; Chapon, L.; Doucet, M.; Draper, N.; Ferraz Leal, R.; Gigg, M. A.; Lynch, V. E.; Markvardsen, A.; Mikkelson, D. J.; Mikkelson, R. L.; Miller, R.; Palmen, K.; Parker, P.; Passos, G.; Perring, T. G.; Peterson, P. F.; Ren, S.; Reuter, M. A.; Savici, A. T.; Taylor, J. W.; Taylor, R. J.; Tolchenov, R.; Zhou, W.; Zikovsky, J., Mantid—Data Analysis and Visualization Package for Neutron Scattering and μSR Experiments. *Nucl. Instrum. Methods Phys. Res., Sect. A* **2014,** *764*, 156-166.
(29) Pratt, F. L.; Blundell, S. J.; Marshall, I. M.; Lancaster, T.; Husmann, A.; Steer, C.; Hayes, W.; Fischmeister, C.; Martin, R. E.; Holmes, A. B., μSR in Polymers. *Phys. B* **2003,** *326* (1), 34-40.
(30) Morris, A. J.; Nicholls, R. J.; Pickard, C. J.; Yates, J. R., Optados: A Tool for Obtaining Density of States, Core-Level and Optical Spectra from Electronic Structure Codes. *Comput. Phys. Commun.* **2014,** *185* (5), 1477-1485.
(31) Cros, A., Silicon Surfaces: Metallic Character, Oxidation and Adhension. *J. Phys. France* **1983,** *44* (6), 707-711.

TOC Graphic